



The behavior observed in the previous figure allows confirming that the periodical exchange of power is due to the coupling between the evanescent fields of the directional coupler. Moreover, it has been observed that the effect of the wall tilt are of extreme importance when designing the directional couplers, since it could lead to significant variations of the coupling length.

5.4.2 ARROW-2D Couplers

On the basis of the simulations done in chapter 4 and the previously measured ARROW-2D waveguides, four different directional couplers based on these structures were fabricated. Distances at which waveguides are parallel range from 1000 to 5000 μm . Fabrication steps used were exactly the same as used for ARROW-2D waveguides and only a different mask configuration was required for the lateral antiresonant structures definition, as shown in table 5.5.

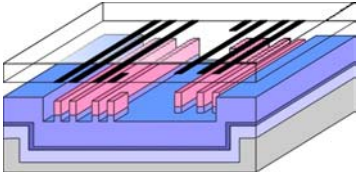
Scheme	Step properties
	<p data-bbox="600 1216 821 1234">CNM-135 M2 mask</p> <p data-bbox="791 1240 858 1258">Mask</p> <p data-bbox="791 1267 1230 1294">Parallel length: 2-5mm in steps of 1mm</p> <p data-bbox="791 1301 1070 1328">Waveguide width: 12μm</p> <p data-bbox="791 1335 1230 1361">Separation between waveguides: 24μm</p> <p data-bbox="791 1368 1289 1395">Lateral antiresonant structures width: 3μm</p> <p data-bbox="791 1402 852 1429">Step:</p> <p data-bbox="791 1435 1059 1462">2μm positive photoresist</p> <p data-bbox="791 1469 1171 1496">1.5μm SiO₂ RIE etching with CHF₃</p>

Table 5.5: Photolithographic step for ARROW-2D directional coupler fabrication.

After the dry etching step, a 2 μm silicon oxide is deposited by PECVD so as to passivate the device from the outer medium. In case of directional couplers, this point is extremely important, since any dust or scratches on the surface could cause a significant variation of the amount of power transmitted to the output waveguide.

In fig. 5.15, the normalized power as a function of the propagation distance is presented either for simulations and experimental results. As can be seen, there exists an important mismatch between them that could be associated to different factors: firstly, no reference waveguide with the same configuration has been designed in the mask (two lateral antiresonant pairs on the outer side and a single lateral antiresonant



structure at the inner side). Secondly, input and output ARROW-2D structures have double lateral antiresonant pairs on both sides, with a variable length that varies from 500 to 2000 μm . Since there were no ARROW-2D waveguides with different lengths available, the attenuation of these waveguides could not be obtained. Both facts do not allow a proper normalization of the power obtained at the device output. As an approximation, results have been normalized to the power at the 12- μm width structure with double lateral antiresonant pair, but clearly this approximation is not satisfactory.

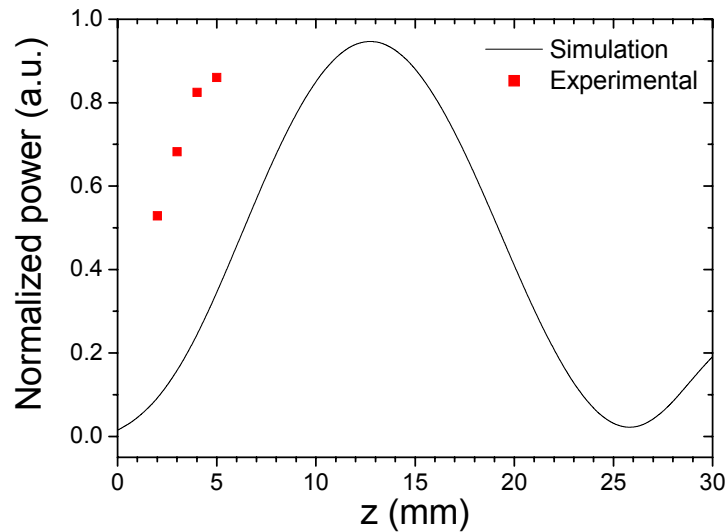


Fig 5.15: Experimental and simulation normalized power at the ARROW-2D directional couplers as a function of the propagating distance.

The near field images of the ARROW-2D directional couplers are shown in fig. 5.16. As can be observed, there exists the expected power transmission to the waveguide output. Then, the remote coupling predicted between distanced waveguides can be confirmed. However, in this case another effect that could have caused small errors during the power measurement at the output waveguide is noticeable: after the region where waveguides are parallel, power remaining in the input waveguide enters into a large (500-2000 μm) slab-ARROW region. Thus, although it still is confined in the y direction, it progressively broadens in the x -axis. Then, power obtained in the ARROW-2D directional couplers with smaller distances could have been overestimated since apart from the light coupled in the directional coupler zone, light propagating through slab-ARROW region could also have reached the output waveguide. In order to



avoid this effect, a modification of the mask where trenches are defined should be made, blocking the input waveguide after the required distance.

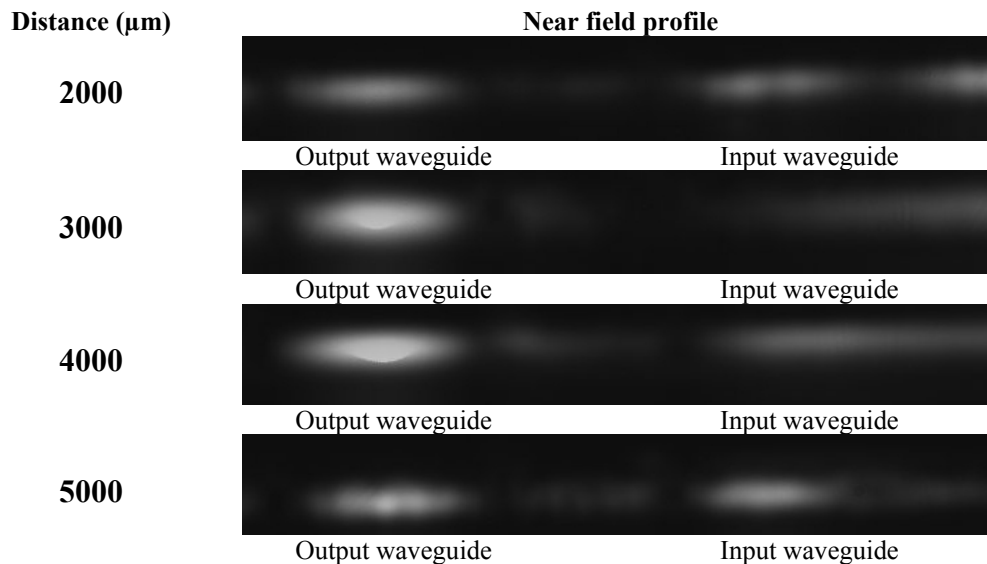


Fig 5.16: Near field profile for ARROW-2D based directional couplers.

Application of ARROW-2D structures to directional couplers has been achieved, confirming the simulations presented in chapter 4. Since attenuation is not known in these structures and there is no reference waveguide on the chip, it is not possible to normalize correctly the experimental results obtained. Remote coupling has been observed in the near-field images, showing the broadening of the light emerging from the input waveguide as it enters in the slab-ARROW zone. This effect should be corrected in the measurements done and prevented in future devices based on ARROW-2D structures.

5.5 3dB Splitters/Junctions

3dB splitter structures based on ARROW structures can be easily obtained using the same technological steps described for rib waveguides but with a different mask, as shown in table 5.6. In order to compare between the different configurations, bent, straight, 1x2 DC and parabolic junctions have been designed. Since it is required that waveguides at the output were single-moded, its width must not exceed 8 micrometers. However, this magnitude in a directional coupler would require an excessively large



length for complete power transfer between waveguides. Thus, in order to compare the different configurations, even thinner waveguides have been chosen, being 5 μ m-width.

	CNM-129 CORE mask: Definition of the rib structure	
		Mask Bent Y-junctions (R=5, 20, 80mm) Straight Y-Junctions ($\alpha=1^\circ$) 1x2 DC. ($d_0=3$ and 4μm) U-junctions (L=5000μm) Waveguide width: 5 μ m total length: 3cm Distance between waveguides: 100 μ m

Table 5.6: Photolithographic step for 3dB splitter fabrication based on ARROW structures.

After the fabrication process, losses as a function of the input fiber optics positions were measured for the Y- and U- junctions with output waveguides of 5 μ m. The main purpose was to analyze the tolerance of these devices to misalignment. As can be observed in fig. 5.17, small displacements of the input fiber optics cause large losses in the Y-junctions. By replacing straight by bend waveguides, a slightly better tolerance and low losses are obtained. However, if a parabolic junction is used, a much better tolerance with misalignment can be observed, together with a significant lowering of the losses. Causes that could lead to this behavior were shown in chapter 4: if a homogeneous wavefront is formed in wide waveguides (in this case the input waveguide was 100 μ m width). Power at the device output would not be as sensitive to misalignments as compared to Y-junctions, where a heterogeneous wavefront, in the form of a single mode, is propagating through the structure.

Another factor that is extremely important in 3dB junctions is the power unbalance, that is, the difference between the power at both waveguides. As can be observed in table 5.17, straight junctions show a large unbalance due to the blunted vertex. The bend junction partially corrects this effect, but a significant unbalance is still observed. By using 1x2 directional couplers unbalance could be reduced to values slightly above 1%, but requires as precise alignment as the bend Y-junctions. On the contrary, with the parabolic junctions, unbalance is reduced at values below 1% with the



previously described alignment tolerance. Again, this behavior can be associated to the homogeneous wavefront on the input waveguide.

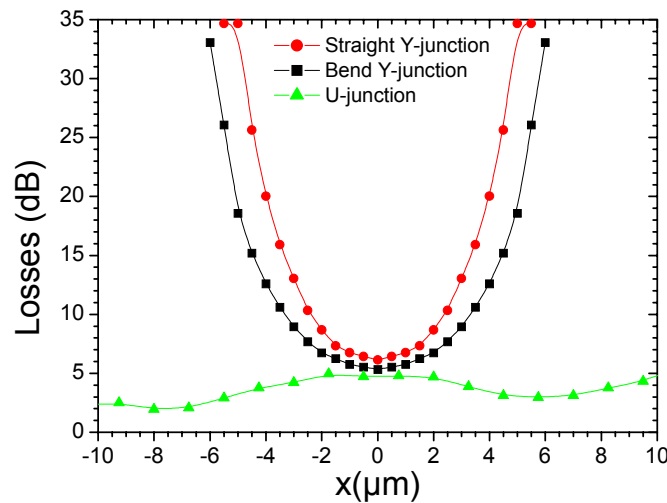


Fig. 5.17: Losses as a function of the input fiber optics misalignment for three different 3dB junctions studied

	Losses in waveguide 1 (dB)	Losses in waveguide 2 (dB)	Unbalance (%)
Straight Y-junction	6.72	6.08	9.54
Bend Y-junction	5.45	5.30	2.72
1x2 directional coupler	6.79	6.71	1.21
U-junction	1.98	1.97	0.83

Table 5.7: Losses in each waveguide of the studied 3dB splitters and power unbalance

It has been observed that both bend and straight Y-junctions require accurate alignment and moreover are suitable to present high unbalance. 1x2 Directional couplers partially correct the unbalance effects, but the accuracy on the alignment is also requested. Only by using U-junctions, high tolerance in the alignment and balance at both branches of the device can be obtained.


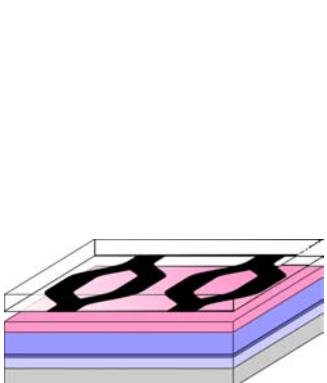
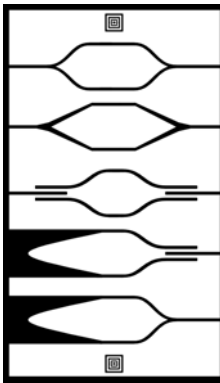
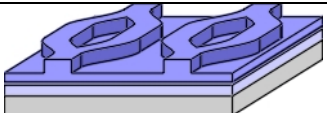

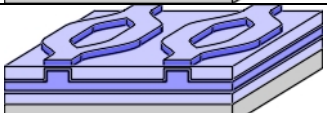
5.6 Mach-Zehnder Interferometers

Technological steps that allow obtaining Mach-Zehnder interferometers are basically identical as those of the waveguides or directional couplers (table 5.8). The only differences arise from the deposition of a very thin LPCVD silicon nitride layer,



Fabrication and Characterization

which allows obtaining a highly sensitive sensor, as it has been previously described and optimized in [2]. After the PECVD silicon oxide passivation, a second mask level is added in order to open the sensing area. As it was described in chapter 2, its length will limit the phase change detection.

Scheme	Step properties	
	Silicon substrate. One-side polished, N-type, 4" diameter, 500 μ m thick 2nd cladding: 2 μ m wet thermal silicon dioxide. n=1.46 1st cladding: 0.38 μ m LPCVD silicon nitride. n=2.00 Core: 4 μ m PECVD silicon oxide. n=1.48	
	CNM-129 CORE mask: Definition of the rib structure 	Mask: Mach-Zehnder Interferometers total length: 3cm Distance between waveguides: 100 μ m Straight Y-Y configuration ($\alpha=1^\circ$) Waveguide width: 4-7 μ m Bent Straight Y-Y configuration (R=5, 20, 80mm) Waveguide width: 4-7 μ m DC-DC configuration ($d_0=3,4\mu$m) Waveguide width: 4, 5 μ m U-DC configuration ($d_0=3,4\mu$m) Input waveguide width: 60, 100 μ m Output waveguide width: 4, 5 μ m U-Y (R=80mm) configuration Input waveguide width: 60, 100 μ m Output waveguide width: 4-7 μ m Step: 2 μ m Positive photoresist
	Rib definition: 2.5 μ m RIE etching with CHF ₃	
	Sensitivity-enhancer layer: 120nm LPCVD silicon nitride n=2.00	
	Passivation: 2 μ m PECVD silicon oxide. n=1.46	



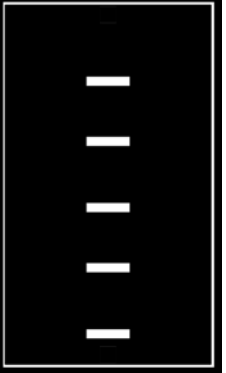
	<p>CNM-129 PROT mask: Definition of the sensor area</p> <div style="display: flex; align-items: center;">  <div> <p>Mask: Sensor area 5-20mm in steps of 5mm</p> <p>Step: 2μm Positive photoresist Passivation opening in sensor area: 2.0μm RIE etching with CHF₃</p> </div> </div>
	<p>Sensitivity-enhancer layer optimization: 80-90nm Si₃N₄ wet etch with H₃PO₄ at 180°C</p>
	<p>Post process: Cutting by a diamond blade Polishing with SIC (0.9μm)+ Al₂O₃ (0.3μm)</p>

Table 5.8: Mach Zehnder Interferometer fabrication steps.

As an example, in fig. 5.18a it can be seen the final appearance of one chip that contains 14 MZI, with straight or bent Y-junctions and single or double sensing regions. It also contains 15 waveguides for reference purposes and 4 Y-junctions, exactly equal to the ones used in the MZI, that allows determining the deviation from the expected 3dB splitting. A detailed picture from the sensing region was taken from an optical microscope and can be seen in fig 5.18b.

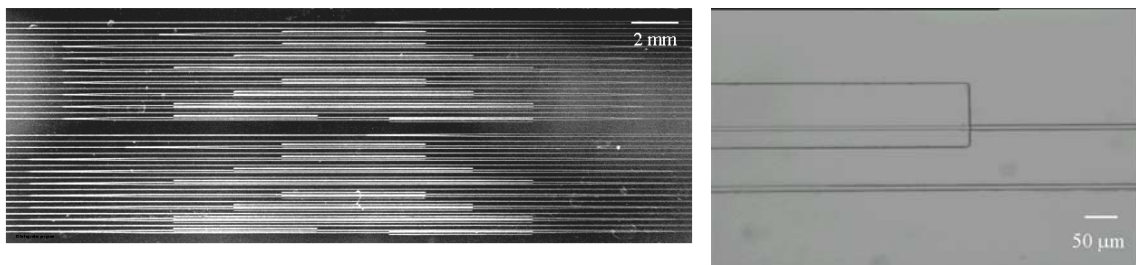


Fig. 5.18: a) Picture of a chip where 14 MZI have been included, together with Y-junctions and waveguides for reference purposes. b) Detail of the sensing region.

Among the several applications where MZI could be used, it has been developed for the detection of biological reactions between two complementary species.



Fabrication and Characterization

Due to the fact that it has been deeply studied and analyzed in [3], the results will be shortened and summarized.

When a biological reaction is produced at the surface of the sensing waveguide, it causes a small variation of its effective refractive index. Thus, MZI surface sensitivity could be determined by injecting a solution with known refractive index on the sensing region. These solutions were different glucose concentrations diluted in deionized water, which allowed refractive index variations at room temperature, as measured by an Abbe refractometer, between 1.3325 and 1.4004 (± 0.0002).

Two essential points are to be obtained from the experimental data: Firstly, the sensitivity should be significantly enhanced with the layer placed between the core and the passivation. Secondly, the MZI should detect very small refractive index variations. For reference purposes, first measurements were done without optimizing the sensing layer, that is, with a silicon nitride layer of 120nm over the waveguide core. Phase changes as a function of the refractive index variation are shown in fig. 5.19. It can be seen that there exists a very small phase change when the refractive index of the outer medium varies. Calculations made from the experimental data proved that the minimum refractive index variation that can be detected with this configuration was $\Delta N = 10^{-4}$. It has to be noted that in order to directly detect a bio-interaction that involves a change in the molecular layer of 10nm, the sensor should be able to detect refractive index variations of $\Delta N = 4 \cdot 10^{-6}$ [4]. Thus, the optical transducer with non-etched sensitive layer will not be able to detect molecular interactions. If this layer is partially etched, just as described in the previous chapter, a significant variation of the phase change can be observed in the same refractive index range as the previous measurements. If this layer is optimized, both simulation and experimental results provide with a minimum refractive index detection of $\Delta N = 1 \cdot 10^{-5}$.